Anal. Chem. **2005,** *77,* 178−184

Si-Supported Mesoporous and Microporous Oxide Interconnects as Electrophoretic Gates for Application in Microfluidic Devices

Riaan Schmuhl,[†] Wietze Nijdam,[‡] Jelena Sekulić,[†] Sankhanilay Roy Chowdhury,[†] Cees J. M. van Rijn,[‡] Albert van den Berg,[§] Johan E. ten Elshof,*[,†] and Dave H. A. Blank[†]

Inorganic Materials Science, MESA+ Institute for Nanotechnology & Faculty of Science and Technology, University of Twente, P.O. Box 217, 7500 AE, Enschede, The Netherlands, Aquamarijn Micro Filtration B.V. Berkelkade 11, NL 7201 JE, Zutphen, The Netherlands, and Laboratory of Biosensors, MESA+ Institute for Nanotechnology & Faculty of Electrical Engineering, Mathematics and Information Technology, University of Twente, P. O. Box 217, 7500 AE, Enschede, The Netherlands

Microfluidic analysis systems are becoming an important technology in the field of analytical chemistry. An expanding area is concerned with the control of fluids and species in microchannels by means of an electric field. This paper discusses a new class of Si-compatible porous oxide interconnects for gateable transport of ions. The integration of such thin oxide films in microfluidics devices has been hampered in the past by the compatibility of oxides with silicon technology. A general fabrication method is given for the manufacture of silicon microsieve support structures by micromachining, on which a thin oxide layer is deposited by the spin-coating method. The deposition method was used for constructing γ-alumina, MCM-48 silica, and amorphous titania films on the support structures, from both water-based and solvent-based oxide sols. The final structures can be applied as microporous and mesoporous interconnecting walls between two microchannels. It is demonstrated that the oxide interconnects can be operated as ion-selective electrophoretic gates. The interconnects suppress Fick diffusion of both charged and uncharged species, so that they can be utilized as ionic gates with complete external control over the transport rates of anionic and cationic species, thus realizing the possibility for implementation of these Si-compatible oxide interconnects in microchip analyses for use as dosing valves or sensors.

The current interest in microfluidics is largely motivated by their envisaged applications. Microfluidic analyses are quickly becoming an established technology in analytical chemistry and biotechnology,[1] and the large potential that microfluidic approaches may offer in the field of synthetic chemistry is only starting to be explored.[2] Microchip-based fluidic devices for chemical analyses or synthesis have several unique advantages over macroscopic approaches, such as a very high degree of temporal control over temperature and chemical environment, high accuracy, relatively easy automation, and integration of functional components such as heaters, temperature controllers, and feeding channels.[3] One of the issues in microfluidic technology concerns the development of selective barriers that allow active control over the transport of specific molecular or ionic species. Switchable interconnects[4] with which certain components can be transported at will from one microchannel into the other may lead to enabling technologies by permitting new ways of molecular separation, improved control over reactions in which one or more reagents have to be dosed in limited quantities, and coupling of methods for molecular identification, where it is necessary to inject small samples for a series of complex chemical manipulations or analysis.[5] Such molecular or ionic gates could be used in chromatography, for instance by collecting samples of bands separated by electrophoresis for further analysis or characterization.

Martin and co-workers were the first to show[6] the concept of influencing the ion permselectivity of gold-plated nuclear track-etched polymeric (Au-NTEP) membranes by imposing a bias

* Corresponding author. E-mail: j.e.tenelshof@utwente.nl. Tel: +31 53 489 2695. Fax: +31 53 489 4683.

[†] Inorganic Materials Science, MESA+ Institute for Nanotechnology & Faculty of Science and Technology, University of Twente.

[‡] Aquamarijn Micro Filtration B.V. Berkelkade 11.

[§] Laboratory of Biosensors, MESA+ Institute for Nanotechnology & Faculty of Electrical Engineering, Mathematics and Information Technology, University of Twente.

(1) Kuo, T.-C.; Sloan, L. A.; Sweedler, J. V.; Bohn, P. W. *Langmuir* **2001**, *17*, 6298−6303.

(2) (a) Edel, J. B.; Fortt, R.; deMello, J. C.; deMello, A. J. *Chem. Commun.* **2002**, 1136−1137. (b) Wang, H.; Nakamura, H.; Uehara, M.; Miyazaki, M.; Maeda, H. *Chem. Commun.* **2002**, 1462−1463. (c) Chan, E. M.; Mathies, R. A.; Alivisatos, A. P. *Nano Lett.* **2003**, *3*, 199−201. (d) Nakamura, H.; Yamaguchi, Y.; Miyazaki, M.; Maeda, H.; Uehara, M.; Mulvaney, P. *Chem. Commun.* **2002**, 2844−2845.

(3) (a) van den Berg, A.; Lammerink, T. S. J. *Top. Curr. Chem.* **1997**, *194*, 21−49. (b) Fintschenko, Y.; van den Berg, A. *J. Chromatogr., A.* **1998**, *819*, 3−12.

(4) (a) Hollman, A. M.; Bhattacharyya, D. *Langmuir* **2002**, *18*, 5946−5952. (b) Nishizawa, M.; Menon, V. P.; Martin, C. R. *Science* **1995**, *268*, 700−702. (c) Kuo, T.-C.; Cannon, D. M.; Chen, Y.; Tulock, J. J.; Shannon, M. A.; Sweedler, J. V.; Bohn, P. W. *Anal. Chem.* **2003**, *75*, 1861−1867. (d) Lee, S. B.; Martin, C. R. *Anal. Chem.* **2001**, *73*, 768−775. (e) Schasfoort, R. B. M.; Schlautmann, S.; Hendrikse, J.; van den Berg, A. *Science* **1999**, *286*, 942−945.

(5) (a) Reyes, D. R.; Iossifidis, D.; Ayroux, P.-A.; Manz, A. *Anal. Chem.* **2002**, *74*, 2623−2636. (b) Ayroux, P.-A.; Iossifidis, D.; Reyes, D. R.; Manz, A. *Anal. Chem.* **2002**, *74*, 2637−2652. (c) Regnier, F. E.; He, B.; Lin, S.; Busse, J. *Trends Biotechnol.* **1999**, *17*, 101−106. (d) Andersson, H.; van den Berg, A. *Sens. Actuators, B* **2003**, *92*, 315−325.

(6) Nishizawa, M.; Menon, V. P.; Martin, C. R. *Science* **1995**, *268*, 700−702.

10.1021/ac049219c CCC: $30.25
Published on Web 12/01/2004

potential on the gold layer of the nanotubule membrane relative to the feed solution. The ion selectivity of the Au-NTEP membrane was dependent on the dimensions of the double layer, i.e., the fluid layer near the pore wall that contains an excess of ions with charge opposite to the natural surface charge that is present on the pore walls. When the double layer is sufficiently thick, overlap inside the pore occurs, so that the entire solution volume in the pore is charged. This situation gives a high anion or cation selectivity and gives the largest change in flux. Lower ion selectivity is observed when double layer overlap is not complete, and a smaller change in flux is observed with applied potential. Under double layer overlap conditions, the Au-NTEP membranes showed bias potential-dependent fluxes for cations, showing higher fluxes at negative bias potentials and lower fluxes at positive potentials. For anions, the opposite trend was observed. The effect of imposing a bias potential to the gold-plated membrane is that the concentration of ions at the membrane interface and inside the membrane pores increases, resulting in enhanced transport of ions by Fick diffusion.[7] Sweedler, Bohn, and co-workers[8] developed a gateable interconnect for analyte injection in microfluidic devices based on an NTEP membrane, where transport was driven by electroosmotic flow (EOF) of the buffer solution through the interconnect, and the selectivity was determined by the double layer overlap in the pore. In contrast to the concept of Martin et al., these interconnects are not ion selective, but they are capable of transporting small volumes of feed solution into an adjacent channel.

In the present work, we developed a new class of selective interconnects with high tunability of diffusion for anionic or cationic species. The interconnect has a silicon-based support structure for mechanical stability, while the selective top layer consists of a thin mesoporous (pore size >2 nm) or microporous (pore size <2 nm) oxide film. The composition, microstructure, and diffusion can be varied at will depending on the targeted function of the interconnect. Of technological importance is the fact that these oxides have higher porosity than NTEP membranes and smaller pore sizes than both anodized aluminum oxide (AAO)[9] and NTEP membranes. The porosity of a membrane is an important factor because it is directly related to the rates of diffusion of species through the membrane. The porosity of NTEP membranes is no more than ~1%, while AAO and oxide membranes have higher porosities, i.e., ~30% for AAO membranes and 50, 53, and 35% for γ-alumina, MCM-48, and titania, respectively. Another important factor is pore size because it determines the intrinsic selectivity of the membrane. In the case of AAO membranes, the minimum pore size is around 10−20 nm,[9] while NTEP membranes can be made with slightly smaller pores. The oxide films we used have average pore sizes in the range of 0.9−10 nm with a narrow pore size distribution, so that double layer overlap can be achieved easily. The principle is demonstrated for

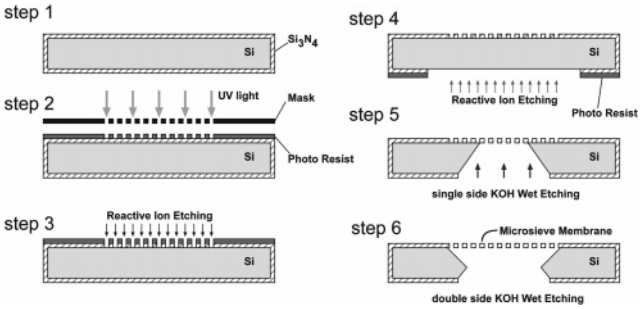

Figure 1. Schematic representation of the processing steps for the microsieve membrane.

mesoporous γ-alumina and template-directed MCM-48 silica,[10] as well as for microporous titania coatings. These thin films can be made inexpensively and easily. The oxide interconnects developed are less than 1 μm thick with pore diameters in the range of 5−8, 2.8, and 0.9 nm, respectively. The pore architectures of the oxide films are all different: γ-alumina has a disordered mesopore structure, MCM-48 has a mesostructured template-directed mesopore architecture, and the titania film is microporous. Because of the silicon support structure, the oxide films can easily be integrated with existing silicon technology. The application of these interconnects as electrophoretic gates is demonstrated. It will be shown that under double layer overlap conditions selective ionic transport can be established by an externally variable potential difference across the interconnect, which allows either cationic, anionic, or no transport depending on the magnitude and sign of the applied potential difference. Results of ion transport experiments are presented here for the three systems, and the influence of applied potential, electrolyte concentration, pH, and pore size on the type and magnitude of transport is discussed.

EXPERIMENTAL SECTION

Materials. Deionized H_2O (18.2 MΩ cm) from a Milli-Q water purification system (Millipore) was used to prepare all solutions. Commercially available reagents were used without further purification. Cetyltrimethylammonium bromide (CTAB), tetraethoxyorthosilicate (TEOS), titanium tetraethoxide, methyl viologen (MV^{2+}), and D-tryptophan (D-Trp) were obtained from Aldrich. Nitric acid (65% solution) and aluminum tri-*sec*-butoxide were obtained from Merck, and poly(ethylene glycol) (PEG) and fluorescein (disodium salt) were from Fluka. Mono- and dibasic potassium phosphate salts used to prepare the buffer solutions were obtained from Fluka and Riedel-deHaën, respectively.

Preparation of Microsieves. The microsieve[11] was made using silicon micromachining. This is schematically represented in Figure 1. A single crystalline silicon wafer (type ⟨110⟩) was coated with a thin layer of low-pressure chemical vapor deposition silicon nitride. At a temperature of 850 °C, a gas mixture of dichlorosilane and ammonia will react and will form silicon nitride. Using an excess of dichlorosilane (70:18), silicon-rich nitride was formed that has less internal stress than stoichiometric nitride and is as such a good membrane material.[12] In step 2, by exposure

(7) Martin, C. R.; Nishizawa, M.; Jirage, K.; Kang, M.; Lee, S. B. *Adv. Mater.* **2001**, *13*, 1351−1362.
(8) Kuo, T.-C.; Cannon, D. M., JR; Shannon, M. A.; Bohn, P. W.; Sweedler, J. V. *Sens. Actuators, A* **2003**, *102*, 223−233.
(9) (a) Vacassy, R.; Guizard, C.; Thoraval, V.; Cot, L. *J. Membr. Sci.* **1997**, *132*, 109−118. (b) Chang, C.-H.; Gopalan, R.; Lin, Y. S. *J. Membr. Sci.* **1994**, *91*, 27−45. (c) van Gestel, T.; Vandecasteele, C.; Buekenhoudt, A.; Dotremont, C.; Luyten J.; Leysen, R.; van der Bruggen, B.; Maes, G. *J. Membr. Sci.* **2002**, *207*, 73−89.
(10) Roy Chowdhury, S.; Schmuhl, R.; Keizer, K.; ten Elshof, J. E.; Blank, D. H. A. *J. Membr. Sci.* **2003**, *225*, 177−186.
(11) van Rijn, C. J. M.; Elwenspoek, M. C. *IEEE Proc. MEMS* **1995**, 83−87.
(12) van Rijn, C. J. M. *Nano and Micro Engineered Membrane Technology*, 1st ed.; Elsevier Press: Amsterdam, 2004.

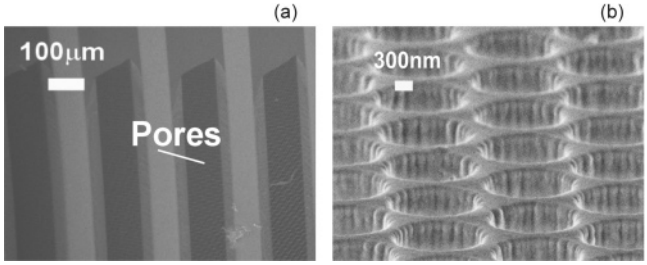

Figure 2. (a) SEM picture of the perforation pattern on silicon nitride microsieves. (b) Overview of uncoated 1.2-μm perforations.

to ultraviolet light, a pattern containing the small openings (1.2 μm or 500 nm) in a mask was exposed using a wafer stepper. After development, the pattern was etched in the silicon nitride using reactive ion etching, with a gas mixture of CHF_3 (25 sccm) and O_2 (5 sccm) at 10 mTorr, 75 W (step 3) for 18 min.

To obtain a free-hanging membrane, the silicon wafer was etched as a support structure by first etching openings from the back of the wafer by lithography and reactive ion etching (step 4). Then by wet etching of KOH, the silicon was removed from the back until the front side of the wafer was reached (step 5); this was done with an etching rate of 1.5 μm min^{-1} for 8.5 h. In the last step, the silicon under the membrane was removed completely. A SEM picture indicating the pattern of perforated areas is shown in Figure 2a and the hexagonal array of circular perforations in Figure 2b. The effective thickness of the perforated area is 1 μm with an overall porosity of 30%.

Preparation of Porous Oxide Interconnects. Silica, titania, and alumina sols were prepared as precursors for the micro- and mesoporous thin films.

(i) Surfactant-templated silica sols were synthesized using the cationic surfactant CTAB and TEOS derived sols.[13] The required amount of TEOS was mixed with 1-propanol and stirred. TEOS was then hydrolyzed by addition of an aqueous HCl solution. 2-Butanol was added to the sol, and the mixture was stirred for another 30 min. The surfactant and water solution was prepared separately and added to the TEOS sol and stirred for 60 min.

(ii) Polymeric titania sols were prepared using titanium tetraethoxide as precursor and nitric acid (65% solution) as acid catalyst to promote the formation of polymeric sols. A given amount of water/nitric acid solution was dissolved in alcohol and added under vigorous stirring to a titanium alkoxide/alcohol solution.[14] The synthesis was performed in a dry nitrogen atmosphere to avoid possible reactions of titanium tetraethoxide with water vapor from ambient air.

(iii) Boehmite sols were prepared by a colloidal sol−gel route, in which aluminum tri-*sec*-butoxide was hydrolyzed in water and subsequently peptized with HNO_3.[15] The boehmite sol was mixed with a PVA solution, in a PVA/boehmite mass ratio of 2:3.

The oxide sols were spin-coated on the silicon nitride microsieves with 500- or 1200-nm perforations. Spin coating was performed under class 1000 cleanroom conditions in order to minimize possible contamination of the wet interconnect layers. The silica layers were dried at room temperature and heated to 450 °C in air for 2 h to calcine the film and remove residual organics. The titania layers were dried in a moisture-free alcohol vapor-saturated atmosphere for 48 h and calcined at 300 °C for 3 h. The boehmite layers were dried in a climate chamber at 40 °C and 60% RH to avoid crack formation in the layer. The γ-alumina interconnects were formed by firing the dried boehmite layers at 600 °C in air. The thickness and quality of oxide layers was checked with HR-SEM (LEO Gemini 1550 FEG-SEM).

Diffusion Measurements. The experimental setup is schematically depicted in one of our earlier articles.[16] The interconnects were placed between the two halves of a U-shaped tube with the oxide layer exposed to the so-called feed side of the interconnect (porous surface area 3.8×10^{-2} cm^2). Aqueous electrolyte solutions (500-mL volume) were added to the feed and receive side cells and stirred vigorously. The pH was regulated with phosphate buffer solutions prepared from mono- and dibasic potassium phosphate salts (pH 6.9 for γ-alumina and pH 7.8 for MCM-48 and titania interconnects) unless stated otherwise. A dc potential difference ΔV was imposed[1] over the interconnect using a potentiostat and external Pt electrodes separated by 4 mm. Here ΔV is defined as $\Delta V = V_{receive} - V_{feed}$, with V_{feed} and $V_{receive}$ the electrode potentials at the feed and receive sides, respectively. ΔV was typically kept between −2 and +2 V to prevent substantial electrolysis of water. All experiments were performed at room temperature. The fluxes were calculated from the concentration changes with time after reaching steady-state conditions. Prior to the experiment, the interconnects were left for 12 h in the receive side electrolyte solution to ensure complete wetting of the oxide layer. Transport experiments were carried out with fluorescein (Fl^{2-}) as divalent anion, D-Trp as zwitterion, and MV^{2+} as divalent cation. Fluorescent probes were analyzed with a BMG Floustar$^+$ (model 403) microplate reader at the excitation (emission) maximum of 488 (510) and 289 (366) nm, respectively, for Fl^{2-} and D-Trp. The detection limit of Fl^{2-} and D-Trp was determined to be 0.1 and 0.5 μM, respectively. Analysis of MV^{2+} was carried out by UV spectroscopy (Agilent Technologies) at 257 nm.

RESULTS AND DISCUSSION

Interconnect Characterization. Figure 3a shows an interconnect with a calcined MCM-48 layer that was deposited on the microsieve by spin coating. The MCM-48 layer penetrated the perforations of the sieve, yielding an average thickness of 970 nm, with a thickness of 650 nm in the center of the perforations. Top and cross-sectional views of microsieves spin-coated with titania and γ-alumina are shown in Figure 3b and c, respectively. Cross sections of the γ-alumina and titania layers spin coated on microsieves reveal that plugs formed inside the perforations, with thicknesses of ∼300 and ∼500 nm for the γ-alumina and titania layers, respectively. To achieve a defect-free γ-alumina layer from the water-based boehmite sol, it was necessary to apply two coatings to overcome surface tension effects that resulted in nonclosed pores after a single coating. This was not necessary for the solvent-based sols where one coating sufficed to form a defect-free layer.

(13) Honma, I.; Zhou, H. S.; Kundu, D.; Endo, A. *Adv. Mater.* **2000**, *12*, 1529−1533.
(14) Sekulić, J.; ten Elshof, J. E.; Blank, D. H. A. *Adv. Mater.* **2004**, *16*, 1546−1550.
(15) Benes, N.; Nijmeijer, A.; Verweij, H. In *Recent Advances in Gas Separation by Microporous Ceramic Membranes*; Kanellopoulos, N. K., Ed.; Membrane Science and Technology Series 6; Elsevier: Amsterdam, 2000; pp 335−372.
(16) Schmuhl, R.; Keizer, K.; van den Berg, A.; ten Elshof, J. E.; Blank, D. H. A. *J. Colloid Interface Sci.* **2004**, *273*, 331−338.

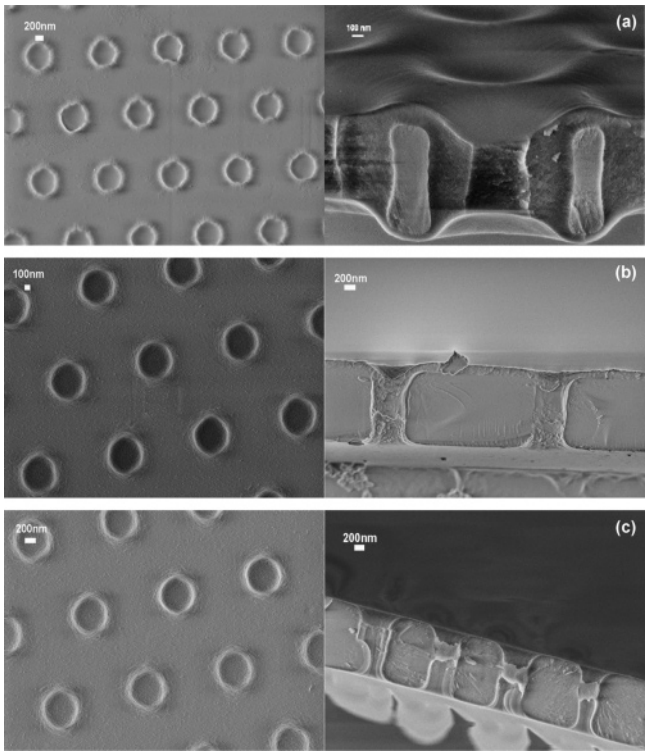

Figure 3. SEM pictures of three different oxide layers spin coated on microsieves with 500-nm and 1.2-μm perforations. Top and cross-sectional views of (a) MCM-48, (b) microporous TiO_2, and (c) γ-alumina layers deposited on microsieves.

The average pore diameter of MCM-48 was determined by nitrogen sorption on unsupported MCM-48 powder and was found to be 2.8 nm. The distribution of Kelvin radii r_K in the supported γ-alumina thin films was determined by the permporometry technique,[17] and the average pore size was found to be in the range of ~5−7.5 nm. The pore size of the titania layer was determined by molecular weight cutoff nanofiltration experiments with PEG solutions,[18] which indicated that the pore size is ~0.9 nm. It is clear that oxide layers with different intrinsic materials properties can be fabricated. Further characterization of the oxides films can be found elsewhere.[19]

Transport Properties. Ion transport experiments were carried out with Fl^{2-}, MV^{2+}, and D-Trp on different types of interconnects. Figure 4a shows the concentration increase of negatively charged Fl^{2-} with time at the receive side after a potential difference ΔV = +2 V had been imposed over the MCM-48 interconnect. However, when $\Delta V \leq 0$, no noticeable concentration increase occurred in 8 h. The opposite trend was observed for positively charged MV^{2+}, as illustrated with a TiO_2 interconnect in Figure 4b.

All molecular and ionic fluxes resulting from electrical potential, concentration gradients, or both are due to one or more of three possible mechanisms of transport: Fick diffusion, ion migration, and EOF. This can be expressed as

$$j_i = j_{F,i}(\nabla c_i) + j_{IM,i}(\nabla V) + j_{EOF,i}(\nabla V) \quad (1)$$

The total flux, j_i of a species type i is expressed as the sum of the three flux contributions, i.e., Fick diffusion $j_{F,i}$, ion migration $j_{IM,i}$, and electroosmotic flow $j_{EOF,i}$, respectively. Equation 2 expresses the Fickian flux $j_{F,i}$ due to a concentration gradient ∇c_i over the membrane.

$$j_{F,i}(\nabla c_i) = -D_i j_{F,i} \nabla c_i \quad (2)$$

where D_i is the chemical diffusion coefficient of species i inside the membrane pores and ∇c_i the concentration gradient. In our experiments, $\nabla c_i \sim c_f/L_m$, with c_f the probe feed concentration and L_m the interconnect thickness (~0.3−1.0 μm). In view of the results shown in Figure 4, the absence of a noticeable flux for all species under field-off ($\Delta V = 0$) conditions at electrolyte strength of 10 mM and a probe feed concentration of 0.8 mM indicates that transport by Fick diffusion was absent under these conditions.

EOF, expressed by eq 3, is driven by the mobile double layer inside the pores and moves the entire liquid under the influence of an electrical potential gradient ∇V.

$$j_{EOF,i} = (\epsilon\zeta/\eta) c_i \nabla V \quad (3)$$

where ϵ is the dielectric constant of the solution inside the pores, ζ the zeta potential[20] of the oxide material, and η the fluid viscosity. In our experiments, $\nabla V \sim \Delta V/L_e$, where L_e is the distance between the electrodes. Since experiments with uncharged D-Trp did not show significant fluxes within experimental error under either field-on or field-off conditions, this suggests that solvent and ion transport by electroosmotic flow is also negligible.

The third contribution, ion migration, is due to an electrical potential gradient over the interconnect, which moves charged species toward the oppositely charged electrode, as expressed by eq 4. Here z_i is the ionic charge of species i, e is the elementary

$$j_{IM,i}(\nabla V) = -(D_i c_i z_i e/k_B T) \nabla V \quad (4)$$

electron charge, k_B the Boltzmann constant, and T the temperature. In Figure 5, the ionic fluxes of Fl^{2-} (ion charge −2) and MV^{2+} (ion charge +2) through different oxide interconnects versus applied potential difference are presented. As can be seen in this figure, the ionic species permeate to electrodes of opposite charge. In all experiments, measurable ionic fluxes were directed toward an oppositely charged electrode at the receive side of the membrane. This shows that the species are transported through the interconnect under the influence of an applied potential gradient and, thus, that the mechanism of transport is ion migration.

The behavior of the interconnects described here differs substantially from the NTEP nanofluidic gates with 15−200-nm channels that were developed by Sweedler, Bohn and co-workers.[1] The transport through their interconnects was dominated by non-ion-selective EOF, which makes them applicable for injection of

(17) Cao, G. Z.; Meijerink, J.; Brinkman, H. W.; Burggraaf, A. J. *J. Membr. Sci.* **1993**, *83*, 221−235.
(18) Puhlfürss, P.; Voigt, A.; Weber, R.; Morbé, M. *J. Membr. Sci.* **2000**, 174, 123−133.
(19) Schmuhl, R.; Sekulić, J.; Roy Chowdhury, S.; van Rijn, C. J. M.; Keizer, K.; van den Berg, A.; ten Elshof, J. E.; Blank, D. H. A. *Adv. Mater.* **2004**, *16*, 900−904.
(20) Hunter, R. J. *Zeta Potential in Colloid Science: Principles and Applications*, 3rd ed.; Academic Press: London, 1981.

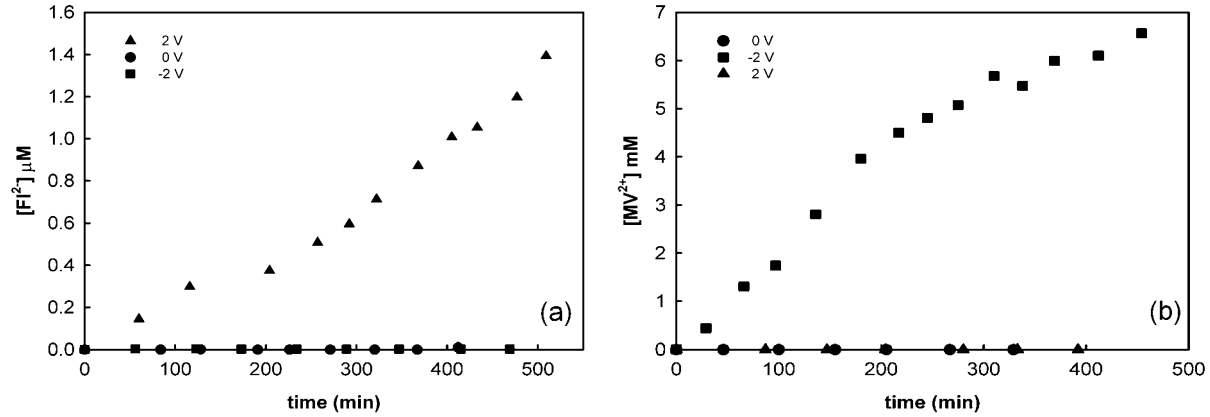

Figure 4. (a) Concentration increase of Fl^{2-} at the receive side versus time, through a MCM-48 interconnect and (b) the concentration increase of MV^{2+} at the receive side versus time through a TiO_2 interconnect. At $\Delta V = -2$, 0, and +2 V. Feed side probe and electrolyte strength concentrations are 0.8 and 10 mM, respectively.

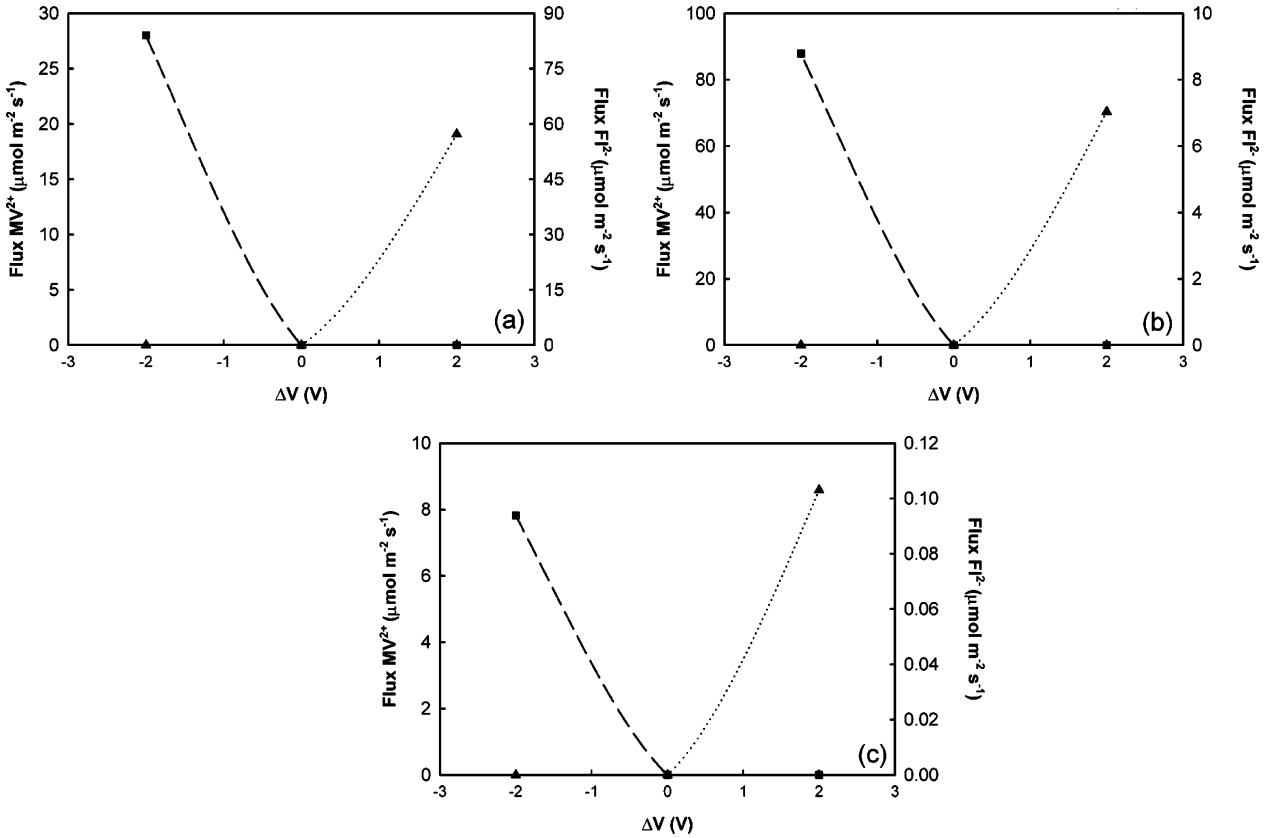

Figure 5. Fluxes of fluorescein (▲, Fl^{2-}) and viologen (■, MV^{2+}) versus electrode potential difference ΔV. Through (a) TiO_2, (b) MCM-48, and (c) γ-alumina interconnect. Drawn lines serve as a guide to the eye. Feed side probe, electrolyte strength concentration, and volume are 0.8 mM, 10 mM, and 500 mL, respectively.

small amounts of analyte solutions from a feed solution into a microchannel. Our interconnects can be used as switchable cation- or anion-selective gates with three stable transfer levels, corresponding with a cation pumping mode, an anion pumping mode, and a closed gate mode. The concept also differs from the ion-permselective Au-NTEP membranes of Martin and co-workers, which operate on the basis of a controlled variation of the concentration gradient over the membrane, thus manipulating the rate of Fick diffusion.

In Figure 6, the effect of electrolyte strength on membrane permselectivity is shown. The electrical double layer theory predicts that as the electrolyte strength increases the double layer thickness decreases. The thickness of the diffuse double layer can be estimated from the Debye screening length κ^{-1}:[15,21]

$$\kappa^{-1} = \sqrt{\frac{\epsilon k_B T}{e^2 \sum_i z_i^2 n_i^0}} \quad (5)$$

where n_i^0 is the number density of ionic species i in the bulk of

(21) Hunter, R. J. *Foundations of Modern Colloid Science*, 2nd ed.; Oxford University Press: Oxford, U.K., 2001.

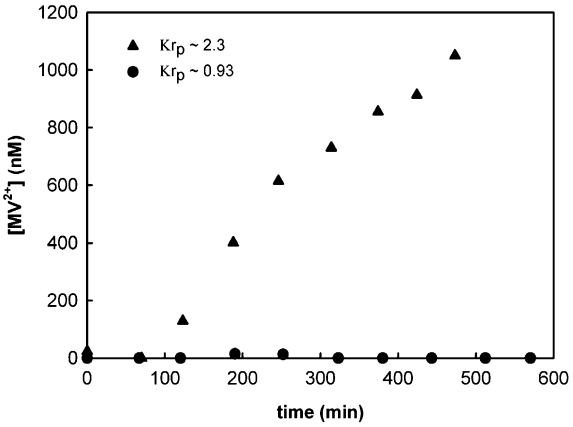

Figure 6. Concentration increase of MV^{2+} at the receive side versus time at $\Delta V = 0$ V, through a MCM-48 interconnect as a function of electrolyte concentration. Feed side probe concentration is 0.8 mM (and volume of 500 mL). $\kappa r_p \sim 2.3$ indicates high electrolyte strength, and $\kappa r_p \sim 0.93$ indicates low electrolyte strength.

the electrolyte solution and $1/2\sum z_i^2 n_i^0$ is the electrolyte strength.[21] The double layer thickness is not constant but decreases with electrolyte strength and increases with surface charge density.[22] When $\kappa r_p < 1$, where r_p is the pore radius, the dimensions of narrow-sized channels approach the length of the double layers and double layer overlap occurs from opposite sides of the pore. Under these conditions, the channel becomes less permeable to ions with the same charge as the surface charge, thus making it a selective barrier for transport of either cationic or anionic species.[23] Alternatively, under conditions at which $\kappa r_p > 1$, the double layer is confined to a small region near the channel wall, and the center of the channel is electrically uncharged, that is, the fluid contains both anions and cations, the total amounts of positive and negative charge being the same. Under these conditions, both cationic and anionic species can be transported through the center of the channel,[21] as shown in Figure 6. This concept of a diffuse double layer holds for pore sizes of >2 nm (mesopores); for pore sizes of <2 nm (micropores), the fluid behavior inside the pores can no longer be described in terms of a continuum approximation, and the transport of species under such conditions will be dominated by the molecular size and shape of the permeating molecule,[24] as well as by dielectric exclusion effects.[25] Since r_p is 1.4 nm for MCM-48, κr_p is ~2.3 at an ionic strength of 0.5 M ($\kappa^{-1} = 0.6$ nm), so that the double layer is confined to a region close to the pore walls, and double layer overlap does not occur. At an ionic strength of 0.01 M, κr_p is ~0.93 ($\kappa^{-1} = 1.5$ nm); i.e., double-layer overlap occurs. The flux of methyl viologen with a feed side concentration of 0.8 mM was measured at both low (0.01 M) and high (0.5 M) electrolyte strength, and the results are shown in Figure 6. Since $\Delta V = 0$ V, any transport should be due to Fick diffusion. No transport of species was observed at low electrolyte strength, while an increase of MV^{2+} occurred at high electrolyte concentration. This clearly shows that the permselectivity of the interconnect is a result of double layer overlap.

(22) Mulder, M., *Basic Principles of Membrane Technology*, 2nd ed.; Kluwer: Dordrecht, The Netherlands, 1996.
(23) Kemery, P. J.; Steehler, J. K.; Bohn, P. W. *Langmuir* **1998**, *14*, 2884−2889.
(24) Bungay, P. M.; Brenner, H. *Int. J. Multiphase Flow* **1973**, *1*, 25.
(25) Lyklema, J. In *Fundamentals of Interface and Colloid Science*, *Vol. 2. Solid−Liquid Interfaces*, 1st ed.; Academic Press: London, 1995; Chapter 5.

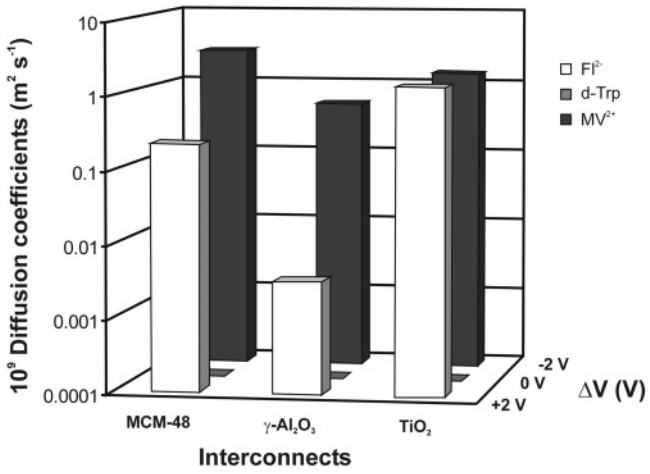

Figure 7. Diffusion coefficients of Fl^{2-}, D-Trp, and MV^{2+}, at given potential differences for different membranes. Transport experiments were done at pH 6.9 for γ-alumina interconnects due to the lack of stability of the γ-alumina layer, at pH 7.8.

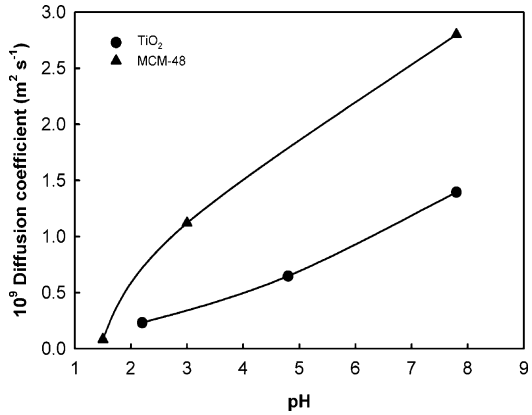

Figure 8. Concentration increase of MV^{2+} at the receive side versus time at $\Delta V = -2$ V through a TiO_2 and MCM-48 interconnects as a function of pH. Feed side probe and electrolyte strength concentrations are 0.8 and 10 mM, respectively. Drawn lines serve as a guide to the eye.

The effective diffusion coefficient D_i of the interconnect toward a species i can be defined by rewriting eq 4.

$$D_i = j_{IM,i} k_B T L_e / c_i z_i e \Delta V \qquad (6)$$

From the flux data presented in Figure 5, the chemical diffusion coefficients can be calculated. The diffusion of Fl^{2-}, MV^{2+}, and D-Trp are shown in Figure 7. It is noted that for MCM-48 the diffusion of MV^{2+} at $\Delta V = -2$ V was much higher than the diffusion of Fl^{2-} at $\Delta V = +2$ V. The same phenomenon occurred in the γ-alumina system, while the diffusion of Fl^{2-} and MV^{2+} in the titania system were similar. The very low Fl^{2-} diffusion in the γ-alumina layer is probably due to strong chemisorption of anions by γ-alumina, resulting in negatively charged pore walls and, thus, in an intrinsically cation-selective layer as shown elsewhere.[16] To explain the behavior of the MCM-48 and titania interconnects, it is necessary to consider the transport of MV^{2+} through the interconnects at constant potential difference and varying pH, as shown in Figure 8. The transport rate of MV^{2+} in the titania interconnect decreased gradually with pH in the range from 7.8

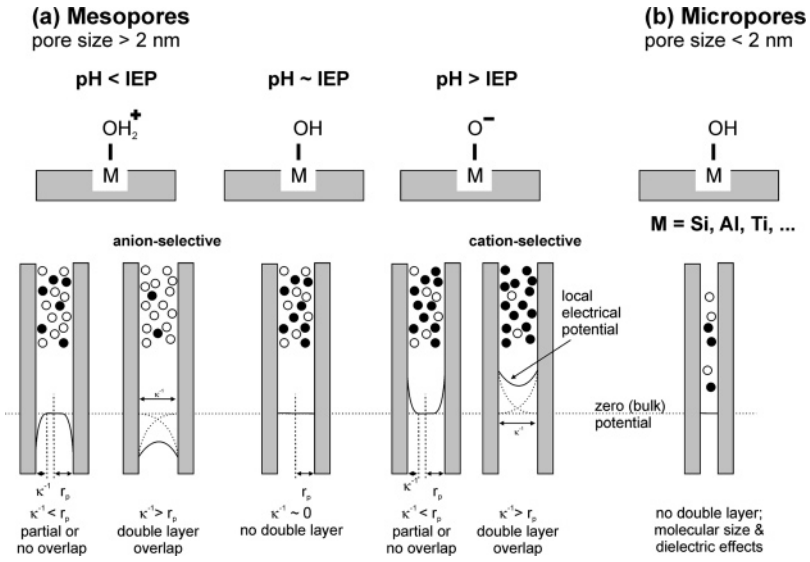

Figure 9. Schematic representation of the surface charge and electrical double layer behavior of micro- and mesoporous interconnects under the influence of pH and electrolyte strength.

to 1.5. The same effect, though much more pronounced, was observed for the MCM-48 interconnect, where the transport rate of MV^{2+} decreased rapidly at pH below 3. The effect of pH on MV^{2+} transport rate can be explained by the surface charging behavior of the two oxides. The isoelectric points (IEP) of silica (IEP = 2−3) and titania (IEP = 4.2−4.8) are well below the pH of 8 at which the experiments shown in Figure 8 were carried out. Hence, the pore walls can be assumed to be effectively negatively charged,[26] so that the counter charges present inside the pores will consist mainly of positively charged ions. On the other hand, at pH below the IEP, the oxide will be positively charged, so that negative counter charges will be dominant in the double layer. This opens up the possibility of tuning the surface charge on the pore walls by changing the pH of the system and thus regulating the nature of the double layer in the pore,[23,27] as illustrated in Figure 9a for the case of the mesoporous MCM-48 and γ-alumina interconnects. As the pH of the solution is gradually lowered, the net surface charge changes from negative to neutral and then to positive. This induces a change in the net charge of the double layer of MCM-48 from positive to negative, leading to a lower transport rate of positively charged species. This explanation is supported by the relatively sharp change of the transport rate of MV^{2+} in MCM-48 at pH below 3 in Figure 8. The transition is observed around pH 2−3, and this is in the same range as the IEP of MCM-48 (silica). Hence, a high cation permeability is expected at pH >3, as was indeed found to be the case for MCM-48. These experiments suggest that the transport rate of anions will be higher at pH <3.

The same phenomenon is less prominent in TiO_2, although the results in Figure 8 show that the trend is qualitatively the same. This and the seemingly non-ion-selective behavior of the titania interconnect for anions and cations as indicated in Figure 7 is most likely related to the microporous nature of this film, which means that diffuse double layer formation cannot occur due to the confined dimensions of the pore, as illustrated in Figure 9b. The transport rate through the titania interconnect is dominated by molecular size, shape, and polarity and by dielectric exclusion effects. Because the molecular sizes of Fl^{2-} and MV^{2+} are in the same range of ~0.9 nm as the pore size of titania, and the molecules are chemically relatively similar, the diffusion coefficients of the two molecules can also be expected to lie in the same order of magnitude. The effect of ionic charge on diffusivity will thus be more modest than for mesoporous systems, and this is reflected by the pH dependency of the titania system in Figure 8.

CONCLUSIONS

A new class of Si-compatible porous oxide interconnects with a silicon microsieve support structure for application in Si-based microfluidic devices has been developed. A general fabrication method for deposition of γ-alumina, MCM-48, and titania oxide layers on micromachined microsieves was demonstrated. In all cases, defect-free interconnects were obtained. Ion transport experiments indicated that these interconnects can be utilized as ion-selective gates through control of electrolyte strength and potential difference over the interconnect. As the interconnects effectively suppress Fick diffusion of charged and uncharged species, they can be utilized as ionic gates with complete external control over the transport rates of anionic and cationic species. The selectivity of the interconnects is achieved by proper choice of electrolyte concentration and pH, while the diffusion is based on molecular size, chemical nature, and ionic charge of the species. This technology can be envisioned in alternative injection techniques, nanocapillary gated injectors for application in microfluidics electrophoretic separations, but also as on-demand therapeutic agents.

(26) Pierre, A. C. *Introduction to Sol−Gel Processing*, 1st ed.; Kluwer: Dordrecht, The Netherlands 1998.
(27) (a) Kang, M.-S.; Martin, C. R.*Langmuir* **2001**, *17*, 2753−2759. (b) Chun, K.-Y.; Stroeve, P. *Langmuir* **2001**, *17*, 5271−5275.

Received for review May 28, 2004. Accepted October 11, 2004.

AC049219C